

Lensing Capillary Waves with a Meniscus

Cade Sbrocco

Department of Physics, Cornell University, Ithaca, New York, 14853

Yukun Sun and Chris Roh*

*Department of Biological and Environmental Engineering,
Cornell University, Ithaca, NY 14853*

Abstract

The propagation of water waves is altered when interacting with curved surfaces. Here, we consider the problem of capillary waves interacting with a 3D meniscus. We show that when capillary waves scatter off an object surrounded by a meniscus, the resulting wavefield can be drastically altered and lensing phenomena is observed. Our results are not only an important step in surface tension dominated wave interactions, but may have implications in the biological communication of surface dwelling animals.

I. INTRODUCTION

The interactions between capillary waves and menisci are fundamentally important to understanding the dynamics of small objects near the capillary length scale (2.71 mm). In nature, surface dwelling organisms may use capillary waves to communicate [1] while abiological floating particles can be propelled and interact through waves in the laboratory [2]. Studies into a meniscus's influence on the scattering of these waves can provide then new insights on the underlying dynamics at play in these systems.

Despite their ubiquity and intimate relationship through surface curvature, there are only a handful of studies that directly investigate the scattering interactions between a meniscus and capillary waves. In 2016, experimental studies investigated how the reflection coefficients depend on the height of pinned menisci at a flat wall [3]. In 2025, complementary experimental and computational studies expanded to considerations of both reflection and transmission coefficients for menisci at shallow, 2D boundaries [4, 5]. These studies were limited to 2D effects, and thus, full 3D scattering pattern incurred by the effect of a meniscus remains to be seen.

The archetypal 3D scattering problem for water waves is that of plane waves incident upon a hard circular cylinder (see Supplemental Material for analytical solution [6]). This problem is generalizable and has been studied in many other wave systems including water surface gravity waves, electromagnetic waves, and acoustic waves, among others. One may alter the scattering with changes in the properties of the cylinder or additional (effective) coatings. For example, with an appropriate depth profile, one may cloak objects from ocean waves [7] and tsunamis are naturally focused by the sloping beaches around islands [8]. For waves at the capillary-gravity scale, surfactant regimes affect the scattering profiles [9] and

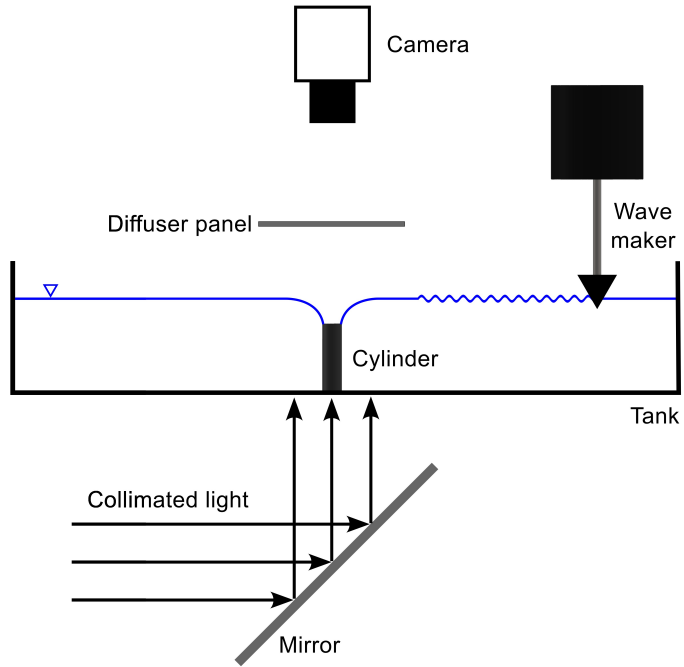


FIG. 1. Schematic of the experimental setup used to obtain shadowgraphs of capillary waves scattering off of a meniscus.

electrostriction of the surface allows for tuneable lenses [10].

In this study, we present the scattering of capillary waves by a meniscus in a 3D system formed around an immersed vertical cylinder. We performed experiments in a wave tank using free-surface shadowgraphy as seen in Fig. 1 to obtain the resulting wavefield amplitudes. We find that a meniscus alters the scattering pattern by acting as an effective media coating an obstacle, similar to the sloping beaches in gravity dominated systems. Both positive and negative menisci can be viewed as converging lenses to varying degrees, lensing water waves into the otherwise shadowed region behind objects.

II. EXPERIMENTAL SETUP

A 60 cm x 36 cm rectangular container filled with water to a depth of 30 mm. A plunger-style wave maker spanning most of the width of the tank and many wavelengths away from the cylinder was attached to a B&K Type 4810 magnetic shaker. This was connected to a Tektronix AFG3101C signal generator in tandem with a B&K Type 2706 power amplifier

to generate continuous, small amplitude, monochromatic capillary waves that were deemed sufficiently planar. The cylinders used as scattering objects were 3D printed out of resin to around 0.05 mm accuracy. For negative menisci, the tops were coated with NeverWet superhydrophobic paint. For positive menisci, a Harrick PDC-32G plasma cleaner was used to activate the surface of the cylinders to decrease the contact angle. The contact line was fixed by pinning the surface to the rim of the cylinder.

We performed shadowgraph measurements by shining collimated light from below the tank with the refracted pattern rear projected onto white diffusing glass (near-Lambertian) a distance 45 mm above the water. A high speed Photron FASTCAM mini AX 200 camera was positioned above the viewing plate to record the pattern at 750 fps with a resolution close to 9.5 pixels per millimeter. When menisci were present, light rays within a distance of $5\ell_c$ of the origin were blocked as to avoid non-physical observation due to caustics (see Supplemental Material for more details [6]. The videos were average subtracted and each pixel was fit to a sinusoid function to obtain intensity amplitudes.

III. PROBLEM STATEMENT

In our otherwise quiescent air-water system, the surface tension σ , fluid density ρ , gravitational acceleration g , and viscosity μ are fixed. A cylinder of radius a with a contact angle φ_c (or equivalently the contact height h_c) uniquely determines a circularly symmetric meniscus profile. With a solid, semi-infinite cylinder (hard), as opposed to a thin disc (translucent), we do not need to consider finite depth or transmission effects. Additionally, pinning the meniscus to the rim of the cylinder allows us to avoid considerations of slip effects [11, 12]. Finally, the incident waves are to be monochromatic (with frequency f , wavenumber k) to avoid dispersive effects, sufficiently within the capillary regime to neglect gravitational effects, planar, and are of small characteristic amplitude ϵ to avoid non-linear effects away from the meniscus [13].

Our system then reduces to five non-dimensional parameters, of which only the first three are effectively tuneable: the contact angle φ_c , the radius $\frac{a}{\ell_c}$, the scattering size parameter $X = ka$, the small characteristic amplitude $\epsilon k \ll 1$, and the fixed Laplace number $\text{La} = \frac{\sigma \rho \ell_c}{\mu^2}$ [14], where $\ell_c = \sqrt{\frac{\sigma}{\rho g}} = 2.71$ mm is the capillary length which will be used as our length scale in all discussions and plots going forward ($\ell_c = 1$).

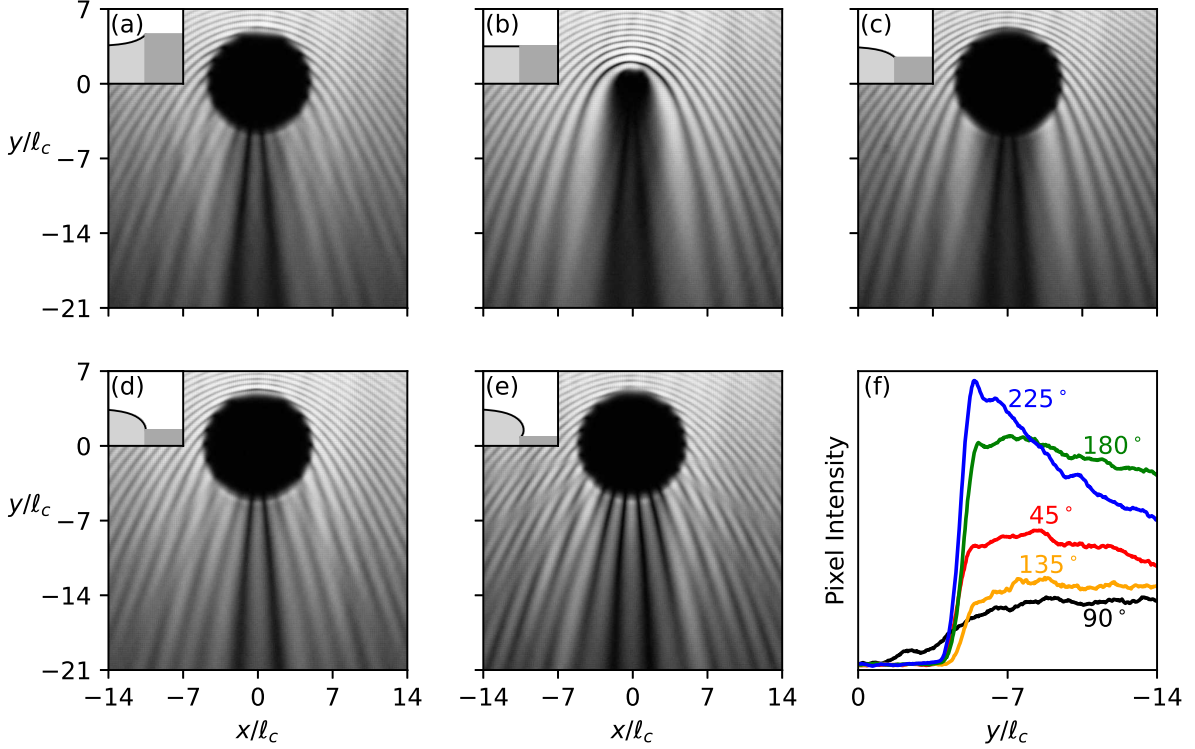


FIG. 2. (a-e) Shadowgraph intensity amplitude fields for menisci of contact angle $\varphi_c = 45^\circ, 90^\circ, 135^\circ, 180^\circ, 225^\circ$, respectively, in arbitrary units. The corresponding meniscus profiles (bold black line) are shown in the inset figures (not to scale). All setups use the same cylinder radius, but for figures (a,c-e) light rays in the shadowgraph incident within a distance $r = 5\ell_c$ of the origin were blocked to avoid possibly non-physical artifacts [6]. (f) Intensity profiles along the centerline of the cylinder. A low pass filter was used to remove noise.

IV. RESULTS AND DISCUSSION

A. Experimental Results

We obtained shadowgraphs for $k \approx \frac{2\pi}{\ell_c}$ ($f = 150$ Hz) waves scattering off of cylinders with varying contact angle and of radius $a = 2\ell_c$ (scattering size parameter $X = 4\pi$). We projected the 3D system onto a 2D screen to obtain images where the pixel intensity of the wave field outside the meniscus roughly corresponds to the surface height (see Supplemental Material for further details [6]). Each pixel's intensity amplitude was found to obtain the total wavefield amplitudes shown in Figs. 2(a-e). To aid in the visualization

of discussed phenomena, the image contrast was increased uniformly across the figures. The raw fitted pixel intensity and phase values are available upon request.

Flat Meniscus ($\varphi_c = 90^\circ$), Fig. 2(b): When no meniscus is present the amplitude field bares a strong resemblance to the ideal hard scattering solution (see Fig. 4 in Section IV C), albeit, with viscous decay. As expected, a mostly shadowed region with minimal illumination due to diffraction is observed directly behind the cylinder. We will use this as our base case for further comparisons.

Positive Meniscus ($\varphi_c = 45^\circ$), Fig. 2(a): If the cylinder is above the mean water level, a positive meniscus forms. As water waves scatter off of the meniscus, we observe a noticeable change in the amplitude field. The meniscus appears to lens the waves to behind the cylinder, illuminating the previously shadowed region. Furthermore, the amplitude profile as a whole is markedly different with additional intensity lobes due to refraction interfering with the diffraction pattern.

Negative Meniscus ($\varphi_c = 135^\circ$), Fig. 2(c): If the cylinder is below the mean water level, a negative meniscus is formed. At the chosen contact angle, the meniscus profile is complementary to the previous positive meniscus. In this case the amplitude field exhibits different behavior to its compliment, showing only a subtle change when compared to the flat meniscus with a slightly more illuminated shadowed region.

Extreme Negative Menisci ($\varphi_c = 180^\circ, 225^\circ$), Figs. 2(d,e): We further increase the contact angle resulting in negative menisci which vertically meet the cylinder and even overturn. Even starker changes in the amplitude field are seen with the furthering increase of the contact angle resulting in more complicated and contrasted features.

To quantify the relative degree of lensing between the cases above, the pixel intensity profiles through the centerline ($x = 0$) of the cylinders are show in Fig. 2(f). The mild negative meniscus does in fact slightly lens the waves compared to the flat meniscus, but not to the same degree as its complimentary positive meniscus. Another feature of note is that the extreme $\varphi_c = 225^\circ$ meniscus appears to focus waves directly into a more localized area behind the cylinder as the amplitude rapidly decreases with distance compared to the other cases.

The narrowing of the shadowed region, additional intensity lobes, and lensing phenomena observed indicate that on average, the menisci slow down the capillary waves in this region, increasingly so with extreme contact angles. Of specific note, a noticeable asymmetry in

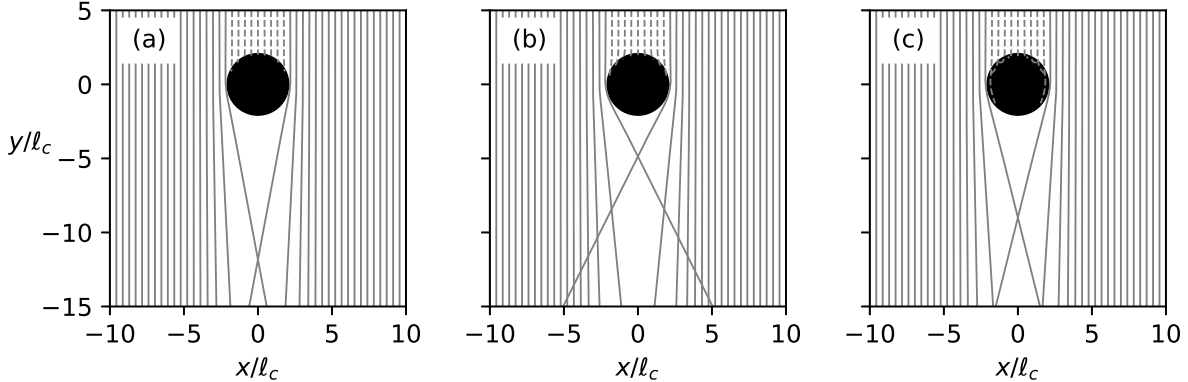


FIG. 3. Geodesics on (a) $45^\circ/135^\circ$, (b) $0^\circ/180^\circ$, and (c) $-45^\circ/225^\circ$ menisci for initially planar rays. Rays which will reflect off of the cylinder are denoted by dashed lines.

behavior is observed between complimentary positive and negative menisci. We liken this overall observed behavior as a capillary analogue to gravity dominated ocean waves being lensed by sloping beaches.

B. Interpretations

To begin identifying the possible mechanisms behind the phenomena observed, we first limit our consideration to waves in the ray limit confined to propagate along a surface S . If the surface appears sufficiently planar such that the dispersion relation remains unchanged across the surface, the ray trajectories must be the geodesics of the surface. While the absolute speed of the wave is unchanging, its projected speed in the xy -plane appears to be slowed (what would be observed in our shadowgraphs). This in itself can result in focusing phenomena, known in the context of gravitational lensing [15] and optical devices [16]. Lensing effects are additionally observed on menisci, strongly refracting glancing and impinging rays as seen in Fig. 3.

These effects are not dependent on the sign of the surface curvature, and thus will be the same for complimentary positive and negative menisci. As such, the asymmetry in our results precludes significant attribution to geodesic effects in the mild menisci. Furthermore, in practice, pure geodesic trajectories will not be observed in our system due to refractive and diffractive effects. However, the waves are still confined to surface and so these effects may be of more importance near the contact line of extreme menisci, albeit obscured.

We now look to identify those physical mechanisms which will affect the dispersion relation (absolute speed) of the waves. Let S explicitly be an air-water interface bounding an inviscid volume V . The dynamic boundary condition of the surface for a small perturbation η is

$$\rho\phi_t = -\sigma\kappa, \text{ on } S \quad (1)$$

where ϕ is the velocity potential and κ is the mean curvature of the perturbed surface. This equation represents the conservation of energy between the inertia and surface tension. The velocity potential due to the geometry is determined by the incompressibility condition

$$\nabla^2\phi = 0, \text{ in } V \quad (2)$$

and the system of equations is complete with the kinematic boundary condition

$$\eta_t = \hat{n} \cdot \nabla\phi, \text{ on } S \quad (3)$$

in addition to any other prescribed boundary conditions. All together, the interplay between the surface tension and inertial effects will determine the wave dynamics. For an infinitely deep system with an otherwise flat surface, the dispersion relation for a wave is

$$c_0 = \sqrt{\frac{\sigma}{\rho}k} = \frac{\text{Surface Tension Effects}}{\text{Inertial Effects}} \quad (4)$$

where c_0 is the phase speed. In cases where there is a curved surface geometry or depth profile, the dispersion relation will be modified in such a way that we can define an index of refraction throughout

$$N_{\text{disp}} = \frac{c_0}{c} = \frac{\text{Inertial Effect Modification}}{\text{Surface Tension Effect Modification}} \quad (5)$$

Only in simple geometries can solutions be analytically found [17], of which our system is not one[6]. In general, N_{disp} can be both greater than or less than unity, complex, inhomogeneous, frequency dependent, and anisotropic.

Modification to Surface Tension Effects: The meniscus and perturbation profiles contribute non-linearly to the surface curvature. Further complexity emerges when the curvature varies sufficiently over a wavelength. These effects are expected to be most relevant in the strongly curved regions near the contact line in extreme menisci. Furthermore, as these effects are independent of the sign of surface curvature, they will affect positive and negative menisci symmetrically.

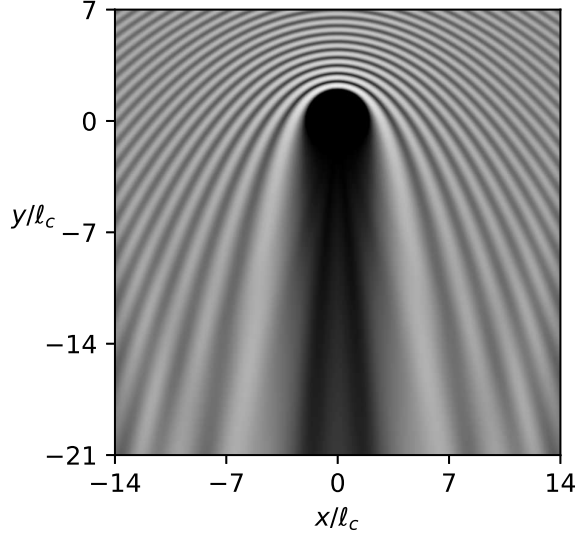


FIG. 4. Simulated wavefield amplitude plot for a bare cylinder with scattering size parameter $X = 4\pi$.

Modification to Inertial Effects: The change in the geometry of a curved surface system will affect how the wave's influence penetrates into the bulk of the fluid. This stems from both the curvature of the surface and, in the case of positive menisci, the finite projected depth between the surface and the cylinder. In contrast to the geodesic and surface tension effects, these effects are dependent on the sign of surface curvature, and thus will affect positive and negative menisci asymmetrically.

It is clear then from the asymmetry between the complementary positive and negative menisci that inertial effects must play an important role in the scattering to result in the observed phenomena. Specifically for mild menisci, this appears to be the dominant mechanism as only the positive meniscus appears to significantly affect the scattering. For the extreme menisci however, the claim of a single important mechanism may be inappropriate and likely requires consideration of inertial, surface tension, and geodesic effects. In other parameter regimes, the interplay between these effects will likely change in addition to possibly requiring consideration of other physical mechanisms (see Supplemental Material for more discussion [6]).

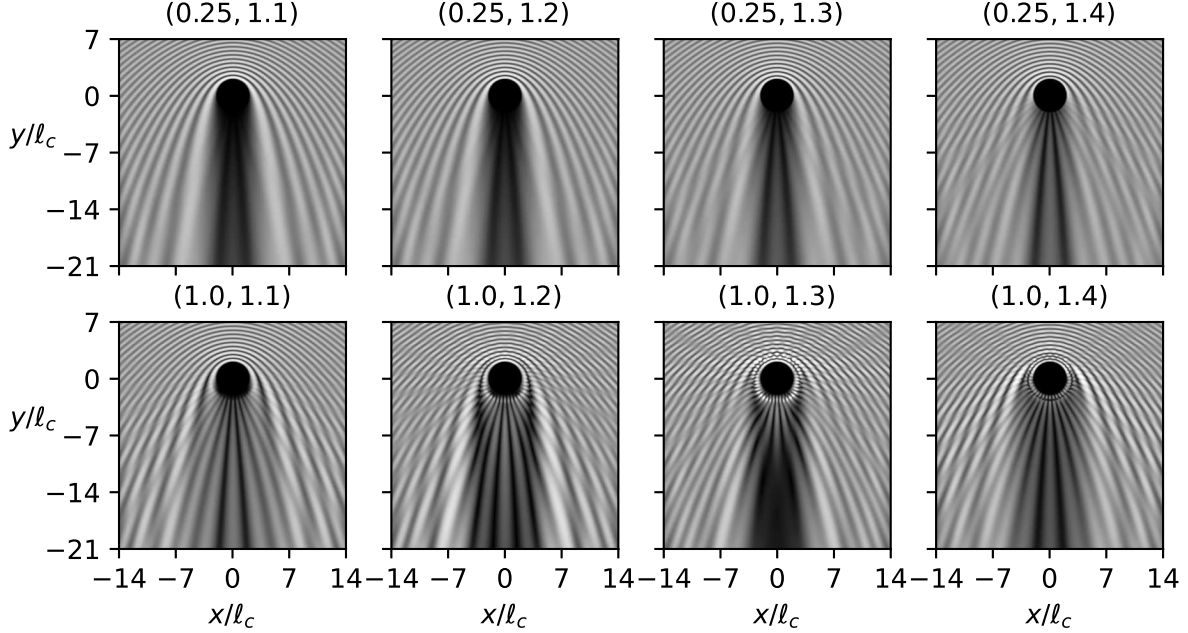


FIG. 5. Various simulated wavefield amplitude plots for coated cylinders (b, N_{coat}) with scattering size parameter $X = 4\pi$.

C. First-Order Model Simulations

We look to see if simpler scattering systems can recreate and aid in interpreting our results. Ignoring pinning, damping, and dispersive effects for simplicity, we use the FDTD solver MEEP [18] to obtain wave amplitude fields to qualitatively compare to our experimental results. We model the menisci, to first-order, as a coating of thickness b with a uniform index of refraction N_{coat} for a system of scattering size parameter $X = ka = 4\pi$. b is interpreted as the extent of the meniscus's influence while N_{coat} is interpreted as the average N_{disp} over this extent.

First, we simulated the bare cylinder case to be compared with our flat meniscus experimental result. The computational result shown in Fig. 4 shows strong qualitative agreement with our experimental result seen in Fig. 2(b) giving confidence in our interpretation of the shadowgraph pixel intensity as the wave height.

We next simulated coated cylinders (b, N_{coat}) , varying over a range of thickness and index of refraction, with the results shown in Fig. 5. Similar trends in structures are observed when compared to our experimental results, which increased intensity lobes and lensing

phenomena. Specifically, the (1.0.1.3) case shows focusing behavior while the (1.0, 1.4) case bares a strong resemblance to our $\varphi_c = 180^\circ$ experimental result in Fig. 2(d).

Trapped modes are observed within the thicker coatings due to $N_{\text{coat}} > 1$ which appear to be the source of the additional intensity lobe structures. This leads us to believe that the meniscus itself may be acting as a waveguide, slowing and guiding the capillary waves to allow for lensing to behind the cylinder. However, there does not appear to be monotonic trends when changing parameters. Our current analysis method precludes determine whether a unique (b, N_{coat}) exists for a given meniscus, and thus we cannot claim if most of the effects occur strongly within a small region close the cylinder or weakly over a larger region. While promising, additional methods of analysis will be needed to investigate the appropriate level of usage of this first-order modeling.

V. OUTLOOK

In this study, we performed experiments to investigate capillary waves scattering off a meniscus in a 3D system. Our experimental results show that the meniscus's presence acts as an effective coating to objects, leading to phenomena such as lensing of the waves behind an obstacle. Across positive and negative menisci, we observe asymmetric behavior but a general trend of a decrease in wave speed. From this, we conclude that inertial effects play a large role in affecting the scattering for positive mild menisci while geodesic, surface tension, and inertial effects likely play a combined role for more extreme menisci.

Beyond cylindrical geometries, one may design novel meniscus profiles formed at membranes [19] and objects of varying shapes [20] which may allow for increase control over capillary wave propagation. Considerations of menisci could also allow for greater insight into studies of interacting, wave-propelled floating particles [2]. Lastly, our results are of relevance to biological communication. Small water surface dwelling animals such as whirligig beetles, water striders, and fishing spiders are known to be highly sensitive to capillary-gravity waves [1]. Our results suggest that the meniscus around these animals may play the role of an abiological lens, allowing for increased perception.

VI. ACKNOWLEDGMENTS

This work was supported by National Science Foundation Grants: NSF-CBET-2442036.

VII. DATA AVAILABILITY

Data is available upon request.

* Contact author: cr296@cornell.edu

- [1] H. Bleckmann, Perception of water surface waves: how surface waves are used for prey identification, prey localization, and intraspecific communication, in *Progress in sensory physiology* (Springer, 1985) pp. 147–166.
- [2] D. M. Harris and J. W. Barotta, Propulsion and interaction of wave-propelled interfacial particles, *Physical Review Fluids* **10**, 100503 (2025).
- [3] G. Michel, F. Pétrélis, and S. Fauve, Acoustic measurement of surface wave damping by a meniscus, *Physical review letters* **116**, 174301 (2016).
- [4] Z. Wang, G. Liu, and L. Zhang, Meniscus-driven modulation of surface wave transmission across a barrier, *Physical Review Letters* **135**, 084001 (2025).
- [5] G. Liu and L. Zhang, Theory of capillary-gravity wave scattering by a fixed, semi-immersed cylindrical barrier with contact line dissipation, *Journal of Fluid Mechanics* **1013**, A27 (2025).
- [6] See Supplemental Material.
- [7] R. Porter and J. Newman, Cloaking of a vertical cylinder in waves using variable bathymetry, *Journal of Fluid Mechanics* **750**, 124 (2014).
- [8] M. Berry, Focused tsunami waves, *Proceedings of the Royal Society A: Mathematical, Physical and Engineering Sciences* **463**, 3055 (2007).
- [9] T. Chou, S. Lucas, and H. A. Stone, Capillary wave scattering from a surfactant domain, *Physics of Fluids* **7**, 1872 (1995).
- [10] V. Mouet, B. Apffel, and E. Fort, Comprehensive refractive manipulation of water waves using electrostriction, *Proceedings of the National Academy of Sciences* **120**, e2216828120 (2023).

- [11] D. Mahdmina and L. Hocking, Scattering of a capillary–gravity wave by a vertical cylinder, *Physics of Fluids A: Fluid Dynamics* **2**, 202 (1990).
- [12] L. Zhang and D. B. Thiessen, Capillary-wave scattering from an infinitesimal barrier and dissipation at dynamic contact lines, *Journal of Fluid Mechanics* **719**, 295 (2013).
- [13] G. Crapper, An exact solution for progressive capillary waves of arbitrary amplitude, *Journal of Fluid Mechanics* **2**, 532 (1957).
- [14] One can equivalently non-dimensionalize as to instead obtain the capillary number $\text{Ca} = \frac{\mu c_g}{\sigma}$, where c_g is the group velocity. One may view this as physically more meaningful than the Laplace number in some contexts since a crude estimate of the rate of decay of capillary waves is $\gamma = 2\text{Ca}k$.
- [15] D. Walsh, R. F. Carswell, and R. J. Weymann, 0957+ 561 a, b: twin quasistellar objects or gravitational lens?, *Nature* **279**, 381 (1979).
- [16] G. Righini, V. Russo, S. Sottini, and G. T. Di Francia, Geodesic lenses for guided optical waves, *Applied Optics* **12**, 1477 (1973).
- [17] L. Rayleigh, On the instability of jets, *Proceedings of the London mathematical society* **1**, 4 (1878).
- [18] A. F. Oskooi, D. Roundy, M. Ibanescu, P. Bermel, J. D. Joannopoulos, and S. G. Johnson, Meep: A flexible free-software package for electromagnetic simulations by the fdtd method, *Computer Physics Communications* **181**, 687 (2010).
- [19] Z. S. Schrecengost, S. Hejazine, J. V. Barrett, V. Démery, and J. D. Paulsen, Shape of a membrane on a liquid interface with arbitrary curvatures, *Physical Review Letters* **134**, 188202 (2025).
- [20] M. Delens, A. Franckart, D. M. Harris, and N. Vandewalle, 3d-printed spines for programmable liquid topographies and micromanipulation, *Nature Communications* **16**, 4348 (2025).

Supplemental Material: Lensing Capillary Waves with a Meniscus

Cade Sbrocco

Department of Physics, Cornell University, Ithaca, New York, 14853

Yukun Sun and Chris Roh*

*Department of Biological and Environmental Engineering,
Cornell University, Ithaca, NY 14853*

S1. FREE-SURFACE SHADOWGRAPHY

The shadowgraphs are a result of light rays incident from below refracting at the water's surface which are subsequently recorded at the viewing plane. Concave and convex regions act as diverging and converging lenses, respectively. For an appropriately placed viewing plane (as to avoid caustics), the light intensity distribution I observed is sensitive to the Laplacian of the optical index of refraction, $\nabla^2 N_o$ [1]. For an otherwise flat two-phase system with small perturbations, the optical index of refraction field is

$$N_o(x, y, z; t) = (N_{o1} - N_{o2})\Theta(\eta - z) + N_{o2} \quad (\text{S1})$$

where Θ is the Heaviside step function. As our disturbance is effectively confined to the xy plane, we find as expected

$$I \propto \nabla^2 N_o|_{z=0} \approx (N_{o2} - N_{o1})\kappa \quad (\text{S2})$$

By use of Eqs. 1-3 in the main text, one can further find that for a monochromatic wave field outside the meniscus, $I \propto \kappa \approx -k^2\eta$. Thus, our observed intensity distribution is representative of the surface height. When a meniscus is present, the complications of caustics are unavoidable due to the strong curvature. We were thus careful to avoid inappropriate analysis of this region which itself oscillates when waves are incident upon it by blocking light rays.

S2. MENISCUS SHADOWGRAPHS

Since the meniscus is a highly curved region, Eq. S2 is not valid for interpreting the surface height in this region. As a result, we are sadly unable to observe the waves themselves on a meniscus with this method. Furthermore, the refraction of light by the meniscus will interfere with the refraction of light elsewhere by the perturbations. We calculate how the rays refract in Fig. S1 showing that an uncensored positive meniscus will create a bright caustic obscuring the cylinder while negative menisci will refract light away creating a shadowed region with a bright outline around the cylinder.

We next plot the final location of the rays upon our viewing screen as a function of their incident position in Fig. S2. From this we determined that a blocker of size $r = 5\ell_c$ is sufficient.

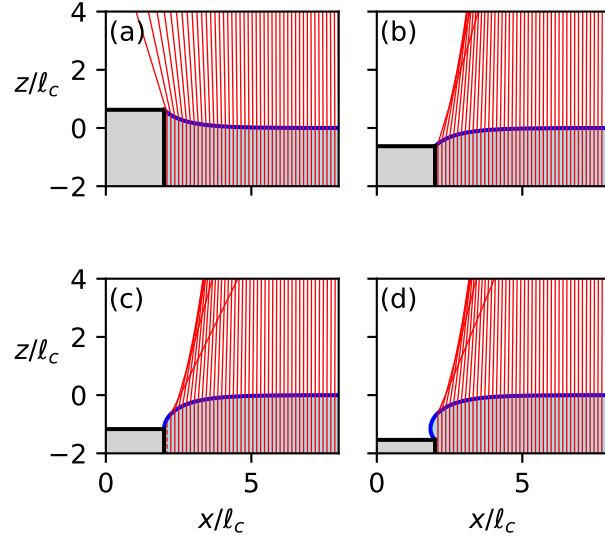


FIG. S1. (a-d) Shadowgraph incident ray trajectories refracting at a meniscus for $\varphi_c = 45^\circ, 135^\circ, 180^\circ, 225^\circ$, respectively.

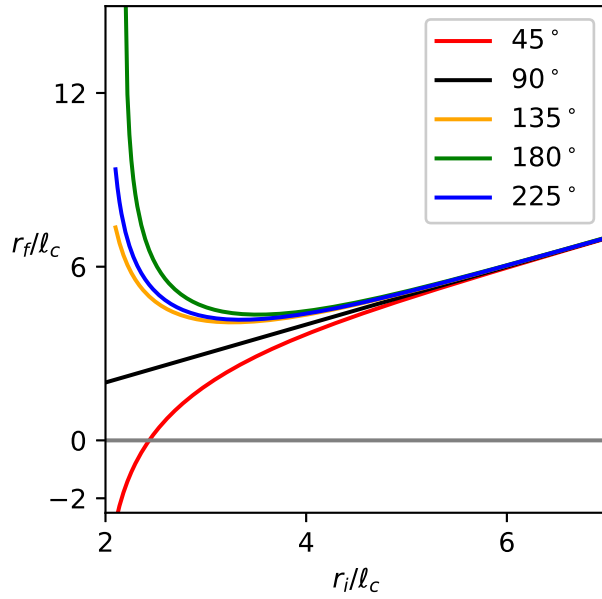


FIG. S2. Shadowgraph incident ray deflections at the viewing screen after refracting at a meniscus. r_i is the incident distance from the origin of the ray while r_f is the final deflected distance from the origin.

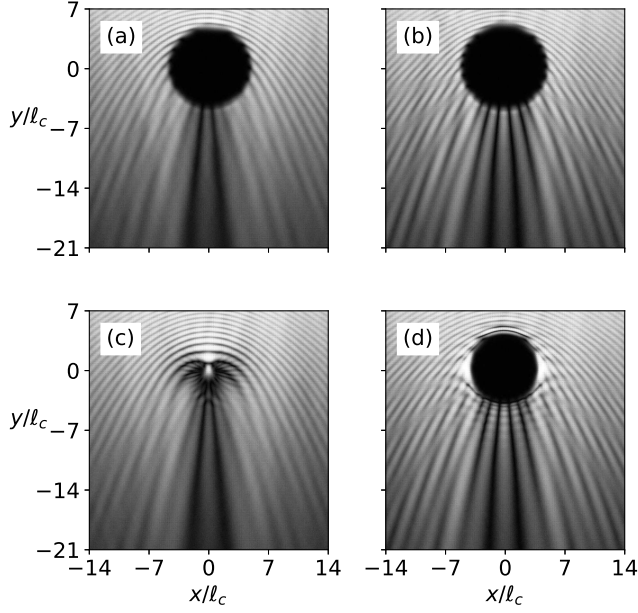


FIG. S3. (a,b) Blocked meniscus shadowgraph amplitude profiles for $\varphi_c = 45^\circ$ and 225° . (c,d) Corresponding unblocked meniscus shadowgraph amplitude profiles.

Lastly, we present the shadowgraph amplitude fields for the $\varphi_c = 45^\circ$ and $\varphi_c = 225^\circ$ menisci when this region is both blocked and unblocked in Fig. S3. We see that there is minimal qualitative change in the features observed far away from the menisci. However, nonphysical artifacts appear near the menisci.

S3. MENISCUS PROFILES

The system of equations in cylindrical coordinates governing the static meniscus's profile h formed around a cylinder of radius a with a contact angle φ_c is

$$h = -\kappa = -\left(\frac{h_r}{r(1+h_r^2)^{\frac{1}{2}}} + \frac{h_{rr}}{(1+h_r^2)^{\frac{3}{2}}} \right) \quad (\text{S3})$$

$$h_r(R) = -\cot \varphi_c \quad (\text{S4})$$

$$h_r(r \rightarrow \infty) \rightarrow 0 \quad (\text{S5})$$

This is a non-linear system of equations which must be solved numerically. To handle overturning menisci, we can re-parameterize the system using $h_r = -\cot \varphi$ [2]. We represent the meniscus as

$$\vec{R}(\varphi, \theta) = (r(\varphi) \cos \theta, r(\varphi) \sin \theta, h(\varphi)) \quad (\text{S6})$$

with our system of equations now as

$$h_\varphi = -\frac{\cos \varphi}{h + \frac{\cos \varphi}{r}} \quad (\text{S7})$$

$$r_\varphi = \frac{\sin \varphi}{h + \frac{\cos \varphi}{r}} \quad (\text{S8})$$

$$r(\varphi_c) = a \quad (\text{S9})$$

$$h\left(\frac{\pi}{2}\right) = 0 \quad (\text{S10})$$

S4. MENISCUS COORDINATE SYSTEM

For our cylindrically symmetric meniscus parameterized by (φ, θ) , the principal curvatures along curves of constant θ and φ are

$$\kappa_1 = \frac{(r_\varphi h_{\varphi\varphi} - h_\varphi r_{\varphi\varphi})}{(r_\varphi^2 + h_\varphi^2)^{\frac{3}{2}}} = \frac{\cos \varphi + hr}{r} \quad (\text{S11})$$

and

$$\kappa_2 = \frac{h_\varphi}{r(r_\varphi^2 + h_\varphi^2)^{\frac{1}{2}}} = -\frac{\cos \varphi}{r} \quad (\text{S12})$$

respectively such that $\kappa = \kappa_1 + \kappa_2$.

Let us now define the orthonormal coordinate system (φ, θ, n) such that a position in space a distance n normal to the surface is

$$\vec{x} = \vec{R} + n\hat{n} \quad (\text{S13})$$

The scale factors in this coordinate system are

$$\lambda_1 = \sqrt{\vec{x}_\varphi \cdot \vec{x}_\varphi} = \left| \frac{1}{\kappa_1} \right| (1 - \kappa_1 n) \quad (\text{S14})$$

$$\lambda_2 = \sqrt{\vec{x}_\theta \cdot \vec{x}_\theta} = \left| \frac{\cos \varphi}{\kappa_2} \right| (1 - \kappa_2 n) \quad (\text{S15})$$

$$\lambda_3 = \sqrt{\vec{x}_n \cdot \vec{x}_n} = 1 \quad (\text{S16})$$

Then, the Laplacian can be expressed as

$$\nabla^2 \phi = \frac{1}{\lambda_1 \lambda_2} \left(\left(\frac{\lambda_2}{\lambda_1} \phi_\varphi \right)_\varphi + \frac{\lambda_1}{\lambda_2} \phi_{\theta\theta} + (\lambda_1 \lambda_2 \phi_n)_n \right) \quad (\text{S17})$$

In general, as is the case for our meniscus, this is a very complicated expression with λ_1 and λ_2 being functions of both φ and n . Furthermore, at sufficient distances from the surface of a negative meniscus, the coordinate system becomes degenerate. After linearization, the incompressibility condition we use to solve for the velocity potential is quite unmanageable and inseparable. Defining the function $f = n - \eta$, the approximation of the perturbed surface curvature $\kappa \approx \nabla^2 f|_{n=\eta}$ will also be quite unmanageable.

S5. GEODESICS ON A MENISCUS

Let $\gamma(t) = (\varphi(t), \theta(t))$ be a geodesic curve on the meniscus where t is the arclength parameter and that for some function $f(t)$, $\dot{f} = \frac{df}{dt}$. By virtue of being on a surface of revolution, the system of equations governing the geodesics is

$$\dot{\varphi} = p \quad (\text{S18})$$

$$\dot{\theta} = q \quad (\text{S19})$$

$$\dot{p} = \frac{rr_\varphi}{r_\varphi^2 + h_\varphi^2} q^2 - \frac{r_\varphi r_{\varphi\varphi} + h_\varphi h_{\varphi\varphi}}{r_\varphi^2 + h_\varphi^2} p^2 \quad (\text{S20})$$

$$\dot{q} = -2\frac{r_\varphi}{r} pq \quad (\text{S21})$$

given an initial position and direction $(\varphi_0, \theta_0, p_0, q_0)$. We can see that Eq. S21 can be directly integrated to obtain a conserved quantity, $L = r_0^2 q_0 = r^2 q$, identified as the angular momentum of the geodesic.

Since a geodesic has unit speed, we can obtain the relation

$$dt = \sqrt{\frac{r_\varphi^2}{\sin^2 \varphi} p^2 + \frac{L^2}{r^2}} = 1 \quad (\text{S22})$$

The apparent speed projected onto the xy plane is

$$ds = \sqrt{\dot{x}^2 + \dot{y}^2} \quad (\text{S23})$$

Using Eq. S22, we find

$$ds = \sqrt{\sin^2 \varphi + \frac{L^2}{r^2} \cos^2 \varphi} \quad (\text{S24})$$

Rays traveling parallel to meridians will experience a large change in apparent speed near the extreme menisci. Additionally, rays more normal to the meridians, far away from the

meniscus, or on mild menisci will have little change in the apparent speed. While we cannot observe pure geodesics in our setup due to multiple limitations, one may be able to imagine a hypothetical experiment in lower gravity perhaps in which observations may be possible.

S6. HARD CYLINDER SCATTERING SOLUTION

In the flat surface case, let us consider the presence of a hard cylinder of radius a in which monochromatic plane waves are incident upon. We will define $a = 1$ to use as our length scale, thus reducing the system to be parameterized solely by the scattering size parameter $X = ka$. Ignoring the pinned contact line boundary condition, we introduce the no-penetration boundary condition at the cylinder:

$$\phi_r(1) = 0 \quad (\text{S25})$$

The process of solving this problem analytically is well established[3], with the resulting wavefield at the surface being:

$$|\eta| \propto \left| e^{iXr \cos \theta} - 2 \sum_0^{\infty} \delta_n i^n \frac{J'_n(X)}{H'_n(X)} H_n(Xr) \cos n\theta \right| \quad (\text{S26})$$

where $\delta_0 = \frac{1}{2}$, $\delta_{n>0} = 1$, J_n is the Bessel function of the first kind, and H_n is the outward propagating Hankel function.

S7. ADDITIONAL MECHANISMS

In different parameter regimes or geometries, other physical mechanisms beyond those considered may play more prominent roles in altering the scattering behavior.

Gravitational Effects: At lower frequencies, gravity's role as a restoring force grows relative to the surface tension. In addition to modifying the dispersion relation directly for the flat surface, there is the added complexity of the restoring force no longer necessarily being normal to the curved surface. As the waves we investigated are of sufficiently high frequency as to be considered pure capillary waves, gravity should only play a role in the formation of the meniscus.

Damping Effects: While the defined N_{disp} in Eq. 5 of the main text does not account for viscosity, the waves do show decay in our results. Already the dispersion relation affected

by viscosity on the flat surface [4], and further viscous effects are known to occur in the meniscus and near the boundary [5, 6]. Specifically for the scattering of capillary-gravity waves, direct measurements of damping effects at pinned menisci are known to significantly alter the reflection coefficient at flat walls [7]. While present in our system, scattering cross-section measurements are likely needed to further investigate its role.

Convective Effects: At sufficiently high amplitude, waves are no longer able to be considered linear, and the propagation of the waves will be affected [8]. Further effects may appear when significant underlying flow is present, alter the propagation of waves and generating steady and unsteady wakes. As our waves are linear and the system is otherwise quiescent, convective effects should be minimal.

Pinning Effects: Enforcing a pinned contact line leads to a singular boundary condition, and thus an additional short range force in the scattering problem [3, 9]. In waveguides [10, 11] and arrays [12], this effect is known to significantly increase the propagation speed compared to non-pinned systems. If this effect was prominent, we would expect to see noticeable signs even in our flat meniscus case. More thorough studies that expand upon our geometry over a range of wavelengths may allow for greater insight into how its role may manifest.

* Contact author: cr296@cornell.edu

- [1] G. S. Settles, *Schlieren and shadowgraph techniques: visualizing phenomena in transparent media* (Springer Science & Business Media, 2001).
- [2] C. Huh and L. Scriven, Shapes of axisymmetric fluid interfaces of unbounded extent, *Journal of Colloid and Interface Science* **30**, 323 (1969).
- [3] D. Mahdmina and L. Hocking, Scattering of a capillary-gravity wave by a vertical cylinder, *Physics of Fluids A: Fluid Dynamics* **2**, 202 (1990).
- [4] G. D. Crapper, *Introduction to Water Waves*, Mathematics and its Applications (Ellis Horwood Ltd, Publisher, Harlow, England, 1984).
- [5] Y. Huang, C. Wolfe, J. Zhang, and J.-Q. Zhong, Streaming controlled by meniscus shape, *Journal of Fluid Mechanics* **895**, A1 (2020).
- [6] R. Kidambi, Meniscus effects on the frequency and damping of capillary-gravity waves in a

brimful circular cylinder, *Wave Motion* **46**, 144 (2009).

[7] G. Michel, F. Pétrélis, and S. Fauve, Acoustic measurement of surface wave damping by a meniscus, *Physical review letters* **116**, 174301 (2016).

[8] G. Crapper, An exact solution for progressive capillary waves of arbitrary amplitude, *Journal of Fluid Mechanics* **2**, 532 (1957).

[9] L. Zhang and D. B. Thiessen, Capillary-wave scattering from an infinitesimal barrier and dissipation at dynamic contact lines, *Journal of Fluid Mechanics* **719**, 295 (2013).

[10] E. Monsalve, A. Maurel, V. Pagneux, and P. Petitjeans, Space-time-resolved measurements of the effect of pinned contact line on the dispersion relation of water waves, *Physical Review Fluids* **7**, 014802 (2022).

[11] J. C. Scott and T. B. Benjamin, Waves in narrow channels: faster capillary waves, *Nature* **276**, 803 (1978).

[12] M. Fauconnier, B. Karunakaran, A. Drago-González, W. S. Wong, R. H. Ras, and H. J. Nieminen, Fast capillary waves on an underwater superhydrophobic surface, *Nature Communications* **16**, 1568 (2025).